surfaces

MDPI

Article

Structural and Antimicrobial Properties of Alginate and Chitosan Films with Silver Nanoparticles

Gabriela Mendes da Rocha Vaz [1,2], Juliana Junqueira Pinelli [1], Cínthia Caetano Bonatto [1] and Luciano Paulino Silva [1,2,*]

[1] Embrapa Recursos Genéticos e Biotecnologia, Laboratório de Nanobiotecnologia (LNANO), Parque Estação Biológica, Final W5 Norte, Brasília 70770-917, DF, Brazil; gabimendvaz@gmail.com (G.M.d.R.V.); jujjpinelli@gmail.com (J.J.P.); cinthiabonatto@gmail.com (C.C.B.)

[2] Postgraduate Program in Biological Sciences (Molecular Biology), University of Brasilia (UnB), Brasília 70910-900, DF, Brazil

* Correspondence: luciano.paulino@embrapa.br; Tel.: +55-61-34484969

Abstract

This study investigates the development and characterization of bioactive films incorporating silver nanoparticles (AgNPs) into biocompatible polymers, namely alginate and chitosan, fabricated using two methods, spin-coating and drop-casting, and aiming to enhance their antimicrobial properties. Dynamic light scattering (DLS) and electrophoretic mobility (EM) of the film precursor solutions revealed significant changes in the nanoparticles' size and Zeta potential (ZP), reflecting the influence of polymer coatings. Alginate contributed to high electrostatic stability due to its negative charge, while chitosan facilitated specific interactions with negatively charged surfaces. Raman spectroscopy revealed that spin-coating conditions did not successfully result in film formation, highlighting the need for further optimization. Therefore, subsequent characterization studies were conducted only for the films formed by drop-casting. Topographical and nanomechanical assessments of these drop-cast films, using atomic force microscopy (AFM) and force spectroscopy, demonstrated that AgNPs reduced adhesion and elasticity in alginate films, while increasing rigidity and adhesion in chitosan-based films. Antimicrobial tests confirmed the efficacy of AgNPs in both precursor solutions and polymer films, with chitosan-based films that retained structural integrity, which makes them suitable for prolonged applications, while alginate films displayed rapid gelation upon hydration, potentially advantageous in short-term applications. The findings underscore the potential of these biopolymer-AgNP composites in creating antimicrobial materials for food packaging, wound dressings, and other biomedical applications. However, challenges related to film deposition methods, such as spin-coating, require further optimization to improve film formation and reproducibility.

Keywords: AgNPs; drop-casting; green synthesis; antibacterial film; Raman spectroscopy; atomic force microscopy

Academic Editor: Aleksey Yerokhin

Received: 9 December 2025
Revised: 17 February 2026
Accepted: 27 February 2026
Published: 1 March 2026

1. Introduction

In recent years, functional biomaterials have gained prominence across various fields, including regenerative medicine, packaging, and biomedical devices, due to their ability to confer specific properties while maintaining biocompatibility, such as antimicrobial activity [1], as well as the controlled release of bioactive compounds [2]. In this context, hybrid polymeric films incorporating nanoparticles have emerged as promising platforms for the

development of multifunctional materials to meet the growing demands of biomedical and industrial applications.

The discussion surrounding the use of biopolymers as alternatives to synthetic plastics has expanded significantly in recent decades, driven by increasing concerns about the environmental impact of synthetic polymers [3]. Industries ranging from food packaging to medical devices, as well as construction and automotive sectors, have recognized biopolymers as sustainable alternatives to conventional plastics [4,5]. In parallel to the rise in biopolymer utilization, nanotechnology has proven to be a crucial tool for modifying and enhancing the functional properties of these materials, facilitating the development of multifunctional systems. Among nanomaterials, silver nanoparticles (AgNPs) stand out for their proven antimicrobial efficacy and their ability to interact with biomolecules due to their high surface area [6]. When incorporated into various matrices, such as biopolymers, AgNPs can exhibit improved colloidal stability and impart antimicrobial properties to the resulting nanocomposite material [7].

Biopolymers such as alginate and chitosan are widely used due to their biocompatibility, biodegradability, and film-forming capabilities [8–10]. Alginate, an anionic biopolymer derived from marine algae, is known for its favorable mechanical and chemical properties that enable interactions with other materials [11]. Chitosan, a cationic polysaccharide derived from chitin, possesses inherent antimicrobial properties [10]. These biopolymers can be processed into films using different techniques, including drop-casting and spin-coating, which can yield distinct morphological and functional characteristics depending on the method employed [12].

The characterization of these hybrid systems, comprising biopolymers and nanoparticles, is essential for understanding the relationship between their physicochemical properties and functional performance. Techniques such as dynamic light scattering (DLS) and electrophoretic mobility (EM) are instrumental in assessing critical solution parameters, including particle size, polydispersity index (PdI), and Zeta potential (ZP). These metrics provide insights into colloidal stability and uniformity, especially for characterizing nanostructures in the early stages of development [13]. Moreover, Raman spectroscopy and atomic force microscopy (AFM) are vital tools for analyzing the chemical structure and morphology of films derived from these solutions [14]. Antimicrobial activity studies further evaluate the efficacy of these materials against target microorganisms [15].

Despite the growing body of research on biopolymer-nanoparticle composites, critical gaps persist in understanding how the choice of film fabrication method (e.g., drop-casting vs. spin-coating) influences the structural, nanomechanical, and ultimately functional properties of alginate and chitosan films loaded with green-synthesized AgNPs. Furthermore, a systematic comparison of how these two biopolymers—with their opposing charges—affect the colloidal behavior of AgNPs in precursor solutions and subsequently modulate film properties and antimicrobial performance remains underexplored. This study addresses these gaps by employing a combined analytical approach (Raman spectroscopy, AFM, force spectroscopy) to directly correlate solution-phase interactions with the physicochemical and antimicrobial characteristics of the resulting films. We selected drop-casting and spin-coating as model techniques because they represent fundamentally different deposition mechanisms (evaporation-driven vs. centrifugal force-driven), allowing us to probe the critical role of substrate adhesion and process dynamics in forming functional bioactive layers from these specific biopolymer-AgNP systems.

In this study, hybrid colloidal suspension of AgNPs combined with alginate and chitosan were developed and characterized by DLS and EM to determine particle size, PdI, and ZP. Bioactive films were produced from these solutions and physicochemically characterized using Raman spectroscopy and AFM. Additionally, antimicrobial activity

studies of both the solutions and the films were conducted to correlate their physicochemical properties with antimicrobial performance, thereby contributing to the development of innovative bioactive materials.

2. Materials and Methods

2.1. Synthesis of Silver Nanoparticles (AgNPs)

Silver nanoparticles (AgNPs) were synthesized using a leaf extract from the native Cerrado plant *Caryocar brasiliense* Camb., under authorization for access to genetic heritage (CGEN no. 02001.007580/2014-95). The synthesis followed the method described by [16], wherein 5 mL of the *C. brasiliense* extract was added to 495 mL of an aqueous silver nitrate ($AgNO_3$) solution at 1 mM concentration (Plat-Lab, Guarulhos, Brazil). The reaction was carried out under dark conditions at 75 °C for 150 min. After synthesis, the AgNPs were characterized by dynamic light scattering (DLS) to assess their size distribution and stored at 4 °C until use.

2.2. Formation of the Polymeric Films

2.2.1. Preparation of Alginate and Chitosan Solutions

Alginate: To prepare a 2% alginate solution, 0.1 g of alginate was dissolved in 5 mL of ultrapure water under magnetic stirring for 1 h. A similar solution was prepared using 5 mL of 1 mM AgNP suspension as the solvent.

Chitosan: A 2% chitosan solution in 0.1% acetic acid was prepared by dissolving 0.1 g of chitosan in 5 mL of 0.1% acetic acid (prepared with ultrapure water) and stirring for 6 h. After 4 h, the acetic acid concentration was adjusted to 0.5% by adding 20 µL of glacial acetic acid. A similar solution was prepared using 5 mL of 1 mM AgNP suspension containing 0.1% acetic acid, which was also adjusted to 0.5% after 4 h.

2.2.2. Substrate Preparation

Circular 6 mm diameter discs of TetraPak laminated packaging were cut using a puncher and treated sequentially: immersion in 0.1% Extran® neutral detergent (Merck KGaA, Darmstadt, Germany) for 5 min, rinsing with ultrapure water for 30 s, immersion in 70% ethanol for 3 min, drying at 80 °C for 5 min, and flattening with gentle manual pressure using the inner surface of Parafilm® (Bemis Company Inc., Neenah, WI, USA).

2.2.3. Film Formation

Drop-Casting: A volume of 40 µL from different solutions was deposited on prepared discs: (i) AgNP 1 mM suspension, (ii) 2% alginate in AgNP, (iii) 2% alginate, (iv) 2% chitosan in AgNP, and (v) 2% chitosan. The films were placed in desiccators and kept at room temperature until complete drying was achieved. They were then stored in desiccators until the subsequent characterization analyses were conducted.

Spin-Coating: A volume of 20 µL of specific solutions was deposited on the discs, rotated at 2000 rpm for 50 s using a homemade spin-coater [17]. The solutions tested were 2% alginate in AgNP, AgNP suspension, and 2% alginate and formed in a homemade spin-coater. The films were stored in desiccators at room temperature until the subsequent characterization analyses were performed.

2.3. Physicochemical and Mechanical Characterization

2.3.1. Dynamic Light Scattering (DLS) and Electrophoretic Mobility (EM)

To characterize the hydrodynamic diameter (HD), polydispersity index (PdI), and Zeta potential (ZP), aliquots of each original formulation—pure alginate, alginate containing AgNPs, pure chitosan, chitosan containing AgNPs, and AgNPs alone—were diluted solely

to achieve the concentration range required for DLS measurements. For each sample, 50 µL of the original suspension were diluted in 950 µL of ultrapure water, maintaining the original polymer-to-AgNP ratio. Measurements were conducted using a ZetaSizer Nano ZS (Malvern, Worcestershire, UK), the HD and PdI were evaluated by dynamic light scattering (DLS), and ZP by electrophoretic mobility (EM). DLS analyses were performed at an angle of 173° using a He-Ne laser (4 mW) at a wavelength of 633 nm. Three measurements were taken of each sample at 25 °C in automatic run mode. The results are presented as the arithmetic mean ± standard deviation of the mean.

2.3.2. Raman Spectroscopy

Drop-cast films were transferred to adhesive tapes on glass slides, and spin-coated films were analyzed directly on cardboard substrates. Spectra were collected using an Alpha 300 RA confocal Raman microscope (Alpha 300 RA, WITec, Ulm, Germany) powered with a TOPTICA diode laser module SYS XTRA 785 nm and 400 mW (TOPTICA Photonics AG, Gräfelfing, Germany) at room temperature. All samples were analyzed under the conditions of single-spectrum acquisition mode using a 100× objective lens, 785 nm filter, and a CCD camera at a temperature of −60 °C, with an integration time of 0.4 s, and a total of 100 accumulations. Three points of each sample were analyzed, and the average was considered to generate the final spectrum. Data were processed using Python libraries (Python 3.13.14, libraries: numpy 2.1.3, matplotlib 3.10.0, scipy 1.15.3) for baseline correction, smoothing, and normalization. The baseline correction was applied to the spectrum using a second-order polynomial fit, subtracting the background trend from the original intensity. After the correction, the data were smoothed using a Savitzky-Golay filter, which reduces noise while preserving signal features, with an 11-point window and a third-order polynomial. The smoothed spectra were then normalized by dividing the intensity by the maximum value, ensuring relative scale comparison between samples. The spectra are plotted with a vertical offset for each sample to facilitate visualization. The 4 (spin-coating) and 10 (drop-casting) largest peaks identified by the spicy find_peaks function were marked in each spectrum.

2.3.3. Atomic Force Microscopy (AFM)

The films formed by drop casting were analyzed at room temperature with an SPM-9600 atomic force microscope (Shimadzu Corporation, Kyoto, Japan) in dynamic mode, equipped with a rectangular cantilever (spring constant of 0.15 N/m and resonance frequency of approximately 24 kHz) integrated with a conical silicon tip. Scans (100 µm^2, 512 × 512 resolution) were performed at 1 Hz, and data were processed with the same manufacturer's software (SPM Manager) for plane leveling and *X*-axis correction, and alignment. Only two regions of each sample were analyzed. After processing, roughness values were obtained, including arithmetic mean roughness (Ra), maximum height (Rz), ten-point height of roughness profile (Rzjis), root-mean-square roughness (Rq), maximum profile peak height (Rp), and maximum profile valley depth (Rv). Finally, all measurements were analyzed by one-way ANOVA and Tukey's test ($p < 0.05$) with Python libraries: matplotlib, numpy, scipy.stats, statsmodels, and pandas.

2.3.4. Force Spectroscopy

Force spectroscopy measurements (force × distance curves) were conducted at ten points using the contact mode of an SPM-9600 atomic force microscope, operated in an atmospheric environment at room temperature. A V-shaped silicon nitride cantilever integrated with pyramidal tips (model TR800PSA, batch 92251B), with a normal flexural spring constant of 0.15 N/m and a curvature radius of approximately 20 nm (Asylum Research—Oxford Instruments, Santa Barbara, CA, USA) was employed. Measurements

were performed in the microscope's online mode, but without full image scanning. The obtained curves were analyzed using the Scanning Probe Image Processor—SPIP™ software (version 5.1.11—Image Metrology), enabling data interpretation and calculation of parameters such as Young's modulus and the energy dissipated during the interaction process. Finally, all data were analyzed by one-way ANOVA and Tukey's test ($p < 0.05$) with Python libraries: matplotlib, numpy, scipy.stats, statsmodels, and pandas.

2.4. Microbiological Assay

To evaluate the antimicrobial activity of the films against *Escherichia coli* (ATCC 8739), a disk diffusion method was performed using Luria-Bertani (LB) agar. The medium was prepared according to the manufacturer's instructions, with agar added at 15 g/L, and autoclaved at 121 °C for 15 min. The bacterial suspension was standardized at 10^8 CFU/mL using a BioPhotometer (model 6131, Eppendorf, Hamburg, Germany), based on the McFarland scale (optical density at 600 nm = 0.5). The inoculum was diluted to 10^7 CFU/mL, and then a 100 µL aliquot was spread onto the agar surface. The films produced by the drop-casting technique, with a diameter of approximately 5 mm, were exposed to ultraviolet (UV) light for 30 min to ensure sterility and were then placed onto the agar surface using sterile tweezers. Additionally, the precursor solutions were tested by depositing 10 µL of each solution onto 6-mm-diameter filter paper disks, which had also been UV-sterilized for 30 min. Control samples included water (negative control), an antibiotic solution containing 10,000 U of penicillin and 10 mg/mL of streptomycin (positive control), and the AgNP stock suspension. The plates were incubated at 37 °C for 72 h, and the inhibition zone diameter was measured at three intervals (24, 48, and 72 h) to evaluate the antimicrobial efficacy of the films and solutions. All experiments were performed in triplicate. The growth inhibition zones were measured using ImageJ software (version 1.53m, National Institutes of Health, USA), and results were expressed as mean ± standard deviation.

2.5. Statistical Analysis

Statistical analyses were performed using one-way analysis of variance (ANOVA) followed by Tukey's post hoc test to assess significant differences between groups at a significance level of $p < 0.05$. The analyses and visualizations were implemented in Python (version 3.8.8) using the numpy, scipy.stats, and matplotlib libraries.

3. Results and Discussion

3.1. Film Formation: Drop-Casting and Spin-Coating Technique

Following the deposition of 40 µL of solution via drop-casting onto the cardboard substrate, a semi-spherical droplet formation was observed. Notably, samples containing AgNP displayed a slightly coppery hue (Figure 1).

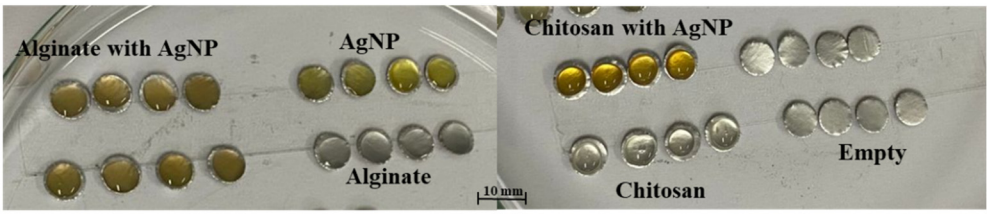

Figure 1. Representative image captured immediately after deposition of 40 µL of each formulation onto substrates. Samples include AgNP, biopolymers (alginate and chitosan), and their respective combinations with AgNP. A control group without any deposition is also shown (Empty).

After 48 h, the deposited films were fully formed and completely dry, as shown in Figure 2. These films appeared visually thin yet cohesive enough to be handled with tweezers. This

outcome suggests that the drop-casting technique efficiently deposited the solutions onto the cardboard surface, resulting in a continuous layer observable to the naked eye. The ability to manipulate the films without damage indicates that the experimental conditions supported the formation of films with sufficient thickness and mechanical integrity.

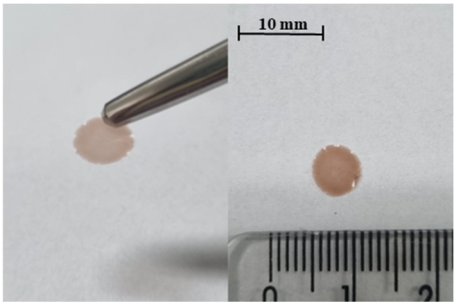

Figure 2. Film formed 48 h after drop-casting. (**Left**): film being gently lifted with tweezers, demonstrating structural integrity. (**Right**): top view of the dried film on a white background, highlighting its shape and uniformity.

In contrast, the spin-coating technique did not produce visually detectable films on the cardboard discs (Figure 3). Even solutions with a coppery coloration—indicative of AgNP presence—failed to yield visible deposits. This discrepancy suggests that the cardboard substrate may exhibit surface characteristics, such as high repellency, that hinder material adhesion. Alternatively, any formed film could have been too thin to be perceptible.

Figure 3. Surface appearance of different formulations after spin-coating. No visually detectable differences were observed among AgNP, alginate, and alginate with AgNP groups.

Overall, drop-casting proved to be a superior method compared to spin-coating under the tested conditions. The use of the selected substrate allowed the films to be easily detached, facilitating their analysis and application. Based on these results, it can be hypothesized that the low interaction between the polymer solution and the cardboard surface contributed to the inefficiency in forming detectable films through spin-coating. The substrate's intrinsic characteristics likely resulted in insufficient adhesion of the polymer material, especially in a technique like spin-coating, where centrifugal force tends to drive the material outward, resulting in a very thin and potentially discontinuous layer. The food-contact surfaces of Tetra Pak packaging, used as a substrate in this study, consist of a thin aluminum layer coated with polyethylene [18]. This surface, engineered for durability and food safety, is both hydrophobic and chemically inert [19]. These properties, while beneficial for packaging purposes, likely posed challenges to adhesion during spin-coating but facilitated the detachment of films formed via drop-casting. This highlights the importance of tailoring film-forming techniques to the properties of both the deposited material and the substrate.

3.2. Characterization

3.2.1. Physicochemical Characteristics of Precursor Solutions

The results summarized in Table 1 and Figure 4 reveal distinct characteristics for the samples analyzed via dynamic light scattering (DLS), including their average hydrodynamic size (HD), PdI, and ZP. AgNP displayed an average size of 183.07 ± 26.35 nm and a PdI of 0.400 ± 0.108, suggesting relatively small, well-dispersed, and homogeneous particles. Their negative ZP (−10.7 ± 1.9 mV) indicates a negatively charged surface, which contributes to colloidal stability through electrostatic repulsion.

Table 1. Hydrodynamic diameter (HD) as Z-average, polydispersity index (PdI), and Zeta potential (ZP) of samples, with values expressed as mean ± standard deviation (n = 3). Statistical analysis was performed using one-way ANOVA followed by Tukey's post hoc test ($p < 0.05$). Significant differences are indicated by: ([a]) AgNP; ([b]) alginate; ([c]) alginate + AgNP; ([d]) chitosan; (*) all groups differ significantly.

	HD (Z-Average) (d. nm)	PdI	ZP (mV)
AgNP	183.07 ± 26.35	0.400 ± 0.108	−10.7 ± 1.9 *
Alginate with AgNP	976.03 ± 126.50 [ab]	0.855 ± 0.212 [a]	−61.6 ± 2.3 *
Chitosan with AgNP	1434.67 ± 184.85 [bd]	0.798 ± 0.084 [abd]	65.1 ± 9.9 *
Alginate	1738.00 ± 297.10 [ac]	0.963 ± 0.064 [a]	−41.9 ± 8.2 *
Chitosan	6778.67 ± 1989.11 [abc]	1.000 ± 0.000 [ac]	52.2 ± 8.5 *

The incorporation of alginate or chitosan into the AgNP suspension resulted in changes in hydrodynamic size, polydispersity, and surface charge (Table 1; Figure 4). Because the polymers were simply mixed with the nanoparticle dispersion, without any additional chemical crosslinking or gelation steps, the observed modifications may be related to physical interactions between the polymers and the AgNPs, such as electrostatic attraction, polymer adsorption onto the nanoparticle surface, and polymer-mediated aggregation. Previous studies using similar approaches—such as the addition of green-synthesized AgNPs (derived from leaf extracts) into chitosan solutions—have reported an increase in hydrodynamic size, particularly under acidic conditions (pH 3), as well as a notable shift in ZP from negative to positive upon polymer–nanoparticle interaction [20].

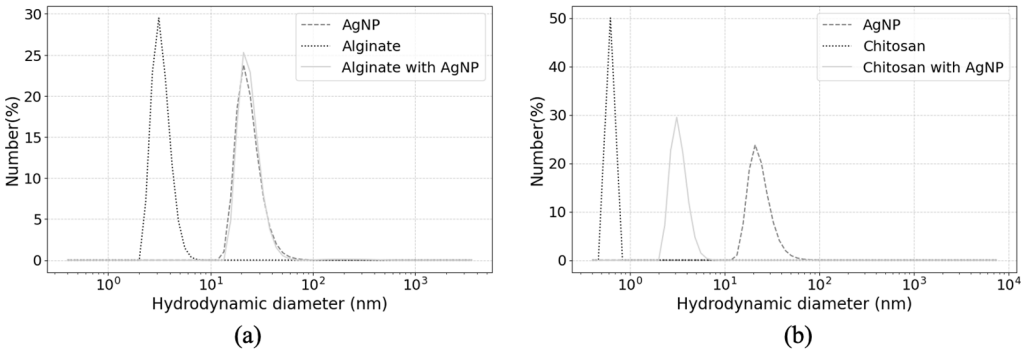

Figure 4. Size distribution (hydrodynamic diameter) as number of nanoparticles. (**a**) Alginate samples and (**b**) chitosan samples.

In this context, it is important to emphasize that the AgNPs used in this study were biosynthesized using a plant extract, which provides a natural source of reducing and stabilizing agents [16]. These biomolecules—typically polyphenols, flavonoids, proteins, and other secondary metabolites—remain adsorbed on the nanoparticle surface as capping agents, imparting distinctive physicochemical characteristics that differ substantially from those of chemically synthesized AgNPs. Such biogenic surface coatings can influence

colloidal stability, interfacial charge, and affinity toward oppositely charged polymers, thereby modulating the extent of polymer adsorption and nanoparticle aggregation. Consequently, the interaction mechanisms observed here between alginate or chitosan and the green-synthesized AgNPs likely reflect not only electrostatic effects but also specific interactions mediated by these plant-derived functional groups, which may contribute to the unique behavior reported in our DLS and ZP analyses.

When alginate was solubilized in the AgNP suspension, the nanoparticles became coated with the polymer, increasing their average size by approximately 792.96 nm. This size increase suggests the formation of polymer layers around the nanoparticles or aggregates formation polymer mediated, which is consistent with the observed rise in increased PdI (approximately 0.455), reflecting greater heterogeneity in the sample. The ZP became more highly negative (-61.6 ± 2.3 mV), indicating strong AgNP–alginate interactions, as alginate carries anionic groups.

Conversely, the mixing of chitosan, a cationic polysaccharide, in the AgNP suspension resulted in nanoparticle coating with this polymer. This process increased the average size of the structures by approximately 1251.6 nm and the PdI by approximately 0.398, indicating the formation of larger and more complex and heterogeneous structures. The positive ZP (65.1 ± 9.9 mV) reflects a surface charge inversion, highlighting possible interactions between the chitosan's cationic groups and the nanoparticles.

The isolated polymer solutions exhibited distinct behaviors in terms of hydrodynamic diameter, with alginate forming smaller structures than chitosan. Both polymers showed PdI values close to 1.0, indicating a high degree of heterogeneity and suggesting extensive aggregation of polymer chains in aqueous suspension. These intrinsic aggregation tendencies likely influence the final physicochemical characteristics observed when the polymers are mixed with AgNPs. Alginate's ZP (-41.9 ± 8.3 mV) suggested moderate stability due to its negative charge. Conversely, chitosan showed a positive ZP (52.2 ± 8.5 mV) implying positively charged particles, though the high size variability may compromise colloidal stability.

In summary, DLS and ZP analyses of the film precursor solutions revealed that alginate and chitosan coatings directly influence the average particle size and ZP. Alginate conferred high electrostatic stability due to its negative charge, whereas chitosan, with its positive charge, changed the AgNP ZP to positive.

3.2.2. Chemical Analysis and Nanoparticle Incorporation in Films

Raman spectra of the spin-coated films showed no significant changes compared to the cardboard substrate, indicating that the deposition did not result in detectable chemical modifications or the formation of consistent layers on the substrate, as evidenced by the same peaks for all samples at 1064, 1129, 1296, and 1445 cm^{-1} (Figure 5). This behavior may be related to the repellent nature of the substrate or the thinness of the generated film, factors that limit the spectroscopic interaction between the deposited material and the Raman beam. Thus, the spin-coating technique, under the tested conditions, was clearly ineffective for this type of surface modification.

The Raman spectra obtained from the analyzed drop-casted film samples are presented in Figure 6. The spectrum of the double-sided tape is characterized by the absence of significant peaks, indicating that this material has a chemically homogeneous composition or lacks Raman features in the spectral range evaluated. This profile serves as a reference for the other spectra, as the samples were deposited onto this substrate.

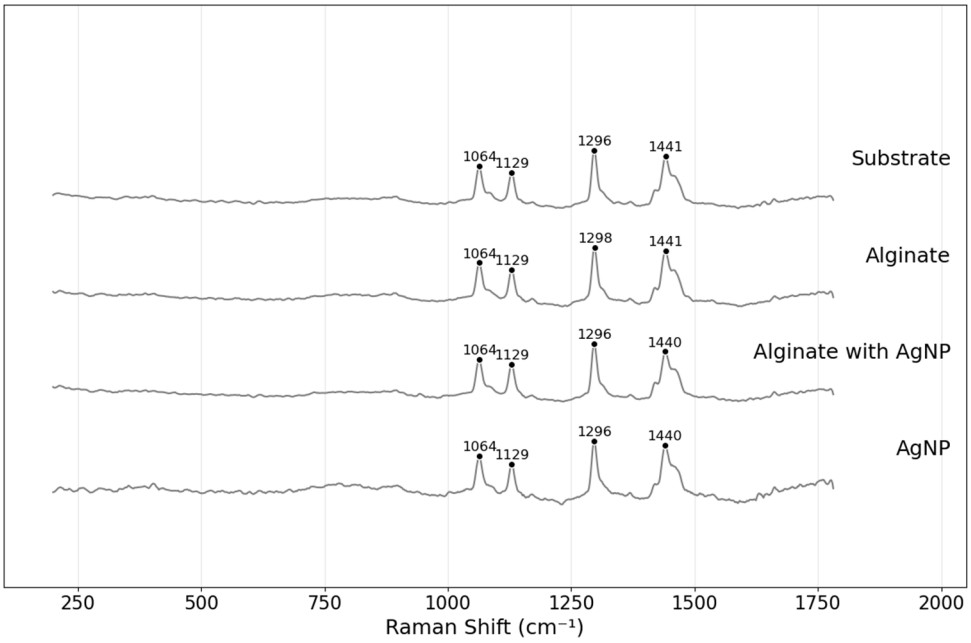

Figure 5. Raman spectra obtained under the same conditions for the different samples produced by spin-coating. The *Y*-axis is offset for the samples to facilitate visualization.

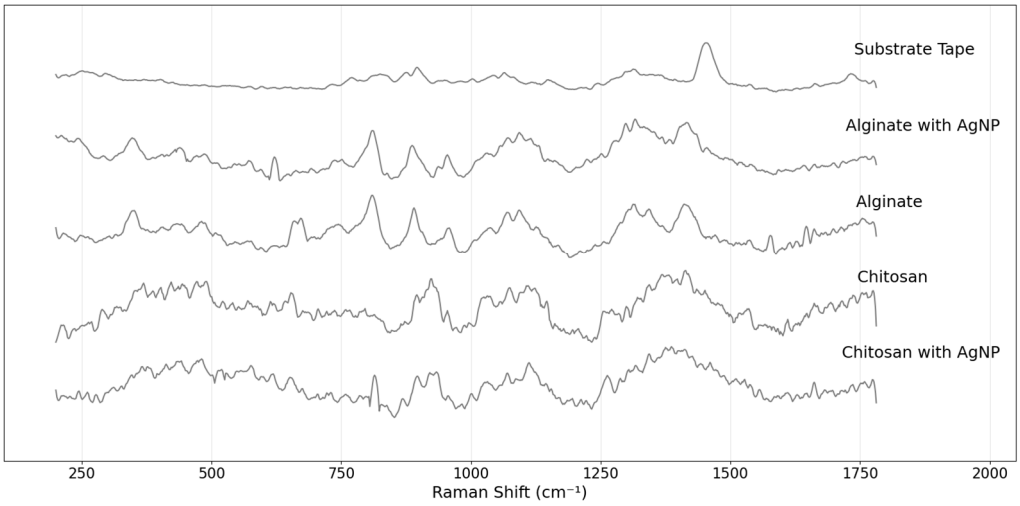

Figure 6. Raman spectra obtained under the same conditions for the different samples produced by drop-casting. The *Y*-axis is offset for the samples to facilitate visualization.

The formed drop-casted films exhibited differentiated properties depending on the polymers and the presence of nanoparticles. For alginate, the addition of AgNPs resulted in films with lower surface roughness, suggesting that the nanoparticles intermingle with the material, filling empty spaces. Raman spectroscopy corroborated the presence of biopolymers and nanoparticles in the films, with characteristic spectral alterations indicating chemical interactions between nanoparticles and polymer functional groups. Peaks attributed to alginate, such as those from carboxylates and hydroxyls, were observed in specific regions, aligning with previous studies [21,22]. For chitosan, the observed peaks correspond to the regions associated with C-C stretching, C-N-H bending, and amine vibrations. These features are consistent with previously reported profiles for pure chitosan in the literature [23,24]. Additionally, the presence of a distinct peak around 814 cm^{-1} exclusively in the chitosan with AgNPs aligns with known spectral signatures of this AgNP [16]. The distinct peak at 584 cm^{-1}, observed in the alginate films containing AgNPs, further

supports the successful integration of these nanoparticles into the polymeric structure, as it corresponds to a characteristic peak identified in the same previous study with this AgNP.

3.2.3. Surface Topography and Roughness of Films

Representative regions from each drop-casted film analyzed by AFM is highlighted in Figure 7. AFM characterization revealed that the chitosan film solubilized in water was more homogeneous and smooth, with gentle elevations and no distinct particles or spots. The overall texture suggests a continuous layer of chitosan, with some prominent points visible in both the topography and phase images, possibly due to polymer aggregation. In contrast, the chitosan film formed from the solution containing AgNPs exhibited a surface with more defined spots and elevated areas, likely corresponding to the presence of the AgNPs. Additionally, distinct viscoelasticities were observed along the film in the phase images. Regarding the alginate films, the AFM analysis confirmed the formation of a homogeneous film with relatively high roughness, but no visually striking differences were observed between the films of alginate solubilized in water or in AgNP suspensions.

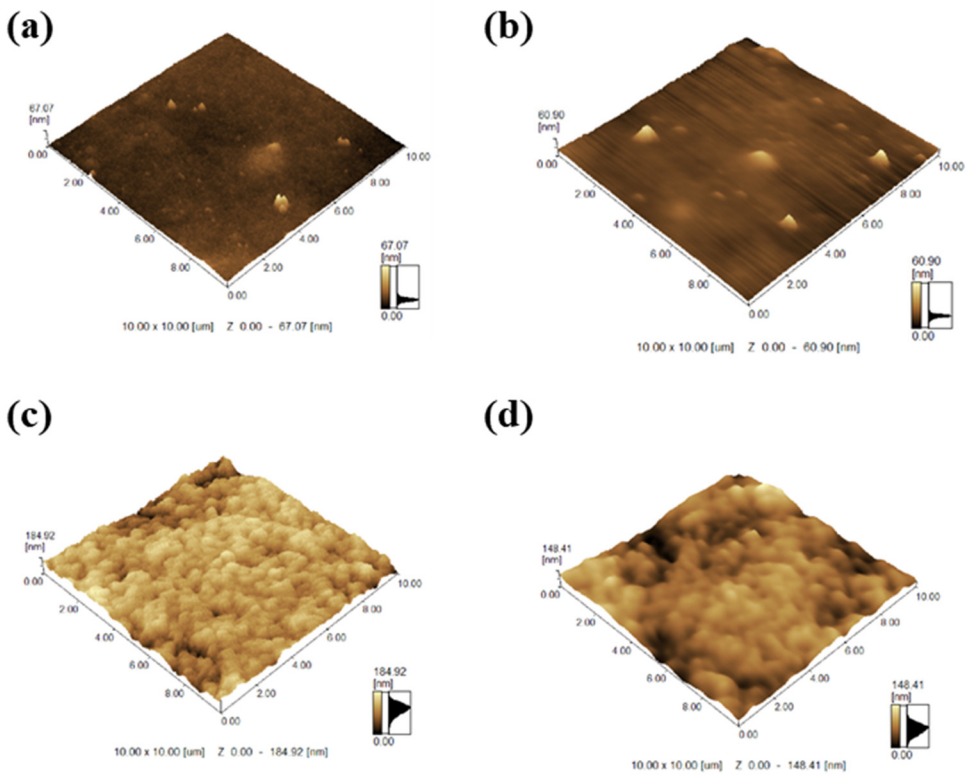

Figure 7. Three-dimensional images of drop-casted films, obtained by atomic force microscopy (AFM) in dynamic mode. (**a**) Chitosan, (**b**) chitosan with AgNPs, (**c**) alginate, and (**d**) alginate with AgNPs.

The topography of the films varied between the polymers, with the most relevant distinctions observed in the presence or absence of AgNPs. The observed morphologies were highly similar to those previously reported in the literature, suggesting that the structural characteristics of the films align well with established studies on polymeric matrices [25–28].

Quantitative parameters obtained from AFM characterization related to surface roughness include Ra (average surface roughness), Rz (arithmetic average of the five highest partial roughness values), Rzjis (a variation of the Rz parameter defined by the Japanese Industrial Standards (JIS)), Rq (root mean square roughness), Rp (average of the heights of the five highest peaks over an evaluation length), and Rv (average depth of the five deepest valleys over an evaluation length). These parameters for each sample can be observed in

Figure 8. The ANOVA results indicate significant differences between the groups for all parameters (Ra, Rz, Rzjis, Rq, Rp, and Rv), with p-values consistently below 0.05, except for the comparison between chitosan and chitosan with AgNP for Rzjis and Rp, where the adjusted p-value was greater than 0.05. The Tukey's HSD post-hoc test confirmed that the inclusion of AgNP in alginate and chitosan formulations significantly affected the measurements in most cases. These findings suggest that AgNP incorporation alters the surface topography of the materials, with notable differences observed across various groups.

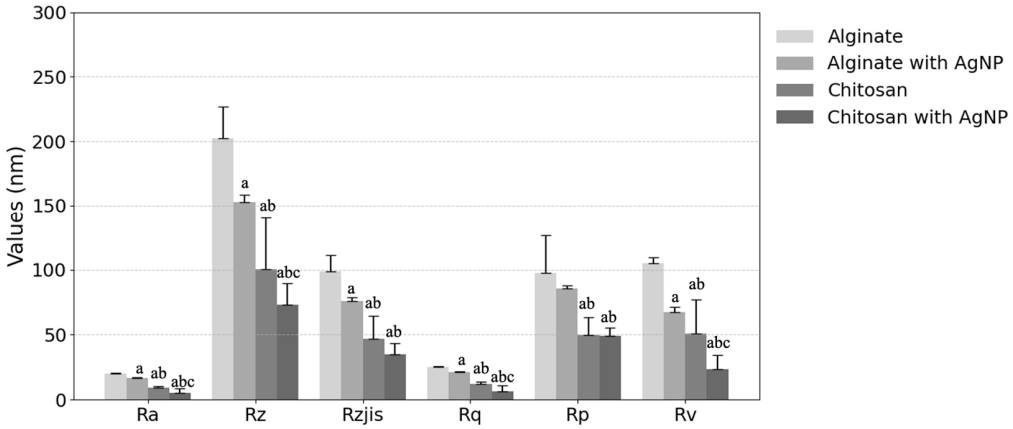

Figure 8. Nanoroughness results obtained by atomic force microscopy (AFM) operating in dynamic mode. Statistical analysis was performed using one-way ANOVA followed by Tukey's post hoc test ($p < 0.05$). Significant differences are indicated by: (a) alginate; (b) alginate with AgNP; (c) chitosan.

3.2.4. Nanomechanical and Adhesive Properties

Figure 9 and Table 2 summarize the results of the force spectroscopy analysis with AFM, which measures different mechanical properties and interactions between the probe and the sample are measured [29]. The parameters reported in nN, where applicable, include the maximum load force, which represents the maximum loading force applied during approach, the maximum pull force, which is the maximum retraction force, the snap-in force, which is the sudden attraction force, and the detach force, which is the detachment force that often shows values similar to the maximum pull force. Other parameters include the Young's modulus, which describes the stiffness of the surface, and the dissipated energy. These data allow for the quantitative characterization of mechanical and adhesive interactions, such as elasticity, adhesion, and energy dissipation during measurements [29].

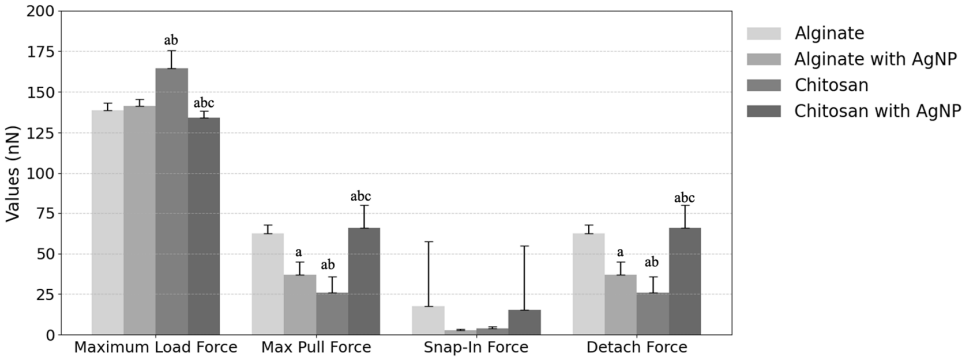

Figure 9. Force spectroscopy results obtained by atomic force microscopy (AFM) operating in dynamic mode. Statistical analysis was performed using one-way ANOVA followed by Tukey's post hoc test ($p < 0.05$). Significant differences are indicated by: (a) alginate; (b) alginate with AgNPs; (c) chitosan.

Table 2. Nanomechanical characterization of the surface of the formed films. Significant differences are indicated by: (a) alginate; (b) alginate with AgNP; (c) chitosan.

	Young's Modulus (MPa)	Dissipated Energy (J)
Alginate	3.67 ± 0.72	$7.11 \times 10^{-15} \pm 1.23 \times 10^{-15}$
Alginate with AgNP	3.68 ± 0.54	$7.63 \times 10^{-15} \pm 1.47 \times 10^{-15}$
Chitosan	3.77 ± 0.82	$7.59 \times 10^{-15} \pm 1.23 \times 10^{-15}$
Chitosan with AgNP	3.85 ± 0.51	$9.07 \times 10^{-15} \pm 2.97 \times 10^{-15}$ abc

Statistical analysis revealed no significant differences ($p > 0.05$) in the Young's modulus (Pa) between the groups, suggesting that the materials (alginate, alginate with AgNP, chitosan, and chitosan with AgNP) have similar mechanical properties regarding this parameter. However, Dissipated Energy (J) shows significant differences between the groups, and Tukey's comparisons indicate that alginate is significantly different from chitosan with AgNP, alginate with AgNP is significantly different from chitosan with AgNP, and chitosan is significantly different from chitosan with AgNP. These results suggest that the incorporation of AgNPs significantly affects the Dissipated Energy of the materials, but does not significantly alter the Z-Young's modulus

Force spectroscopy parameters reflect interactions between the AFM probe and the sample surface, and are useful for assessing elasticity and adhesion [29]. Force spectroscopy analysis provided additional insights into mechanical parameters. As shown in Figure 9, the maximum pull force and detachment force of alginate were reduced in the presence of nanoparticles, suggesting lower adhesion and elasticity, likely due to the interaction of AgNPs with the polymer functional groups. For chitosan, the increase in these parameters indicates greater rigidity and adhesion, possibly due to the integration of nanoparticles into the polymer matrix.

3.3. Antimicrobial Efficacy of Solutions and Films

The alginate films, both with and without silver nanoparticles (AgNPs), exhibited rapid water absorption and transitioned into a gel state shortly after being placed on the agar plates (Figure 10). Alginate films gelled immediately and lost their shape upon contact with the agar, a common behavior for non-cross-linked alginate, due to its inherent gelation properties [30,31]. Despite this, alginate films containing AgNP still exhibited antimicrobial activity in the presence of AgNPs, consistent with previously reported findings [32]. Notably, the gel formed from the alginate solution with AgNPs exhibited antimicrobial activity against *E. coli* at all evaluated time points (24, 48, and 72 h), whereas the alginate gel without nanoparticles showed no significant antimicrobial effect. To ensure their usability in applications where structural stability is vital, further optimization of the film formation process would be necessary.

In contrast, the chitosan films retained their well-defined shape without noticeable water uptake, which enabled the measurement of the inhibition zone by the disk diffusion method (Table 3). Among them, only the film containing AgNPs exhibited clear antimicrobial activity, evidenced by the presence of a small inhibition halo surrounding the film, as shown in Figure 10. This structural stability is particularly advantageous for applications such as food packaging or wound dressings, where maintaining film integrity is essential. Moreover, the antimicrobial response observed in the chitosan–AgNP film is consistent with previous findings regarding the synergistic antibacterial properties of silver nanoparticles incorporated into chitosan matrices, further reinforcing the potential of this composite system for biomedical and preservation-related applications [33].

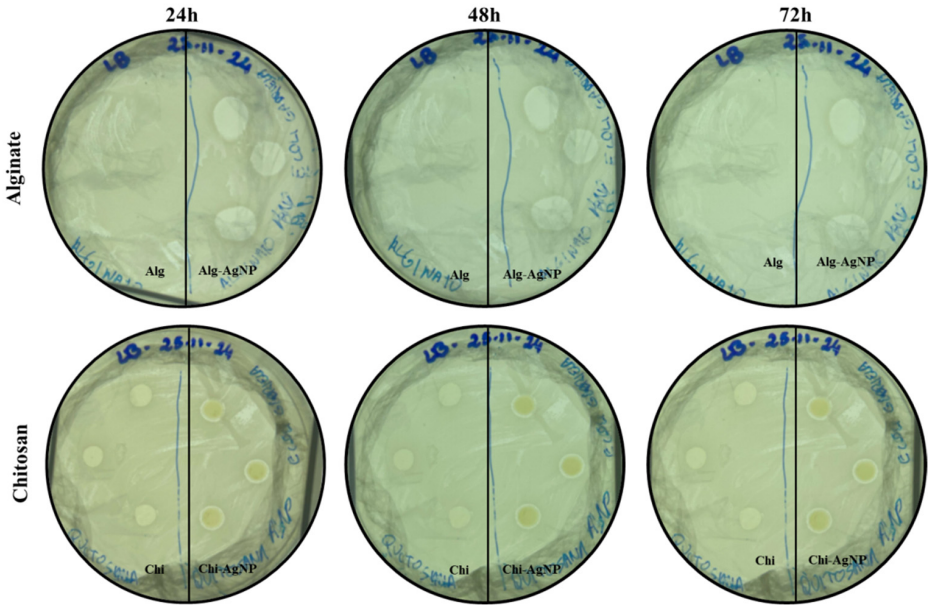

Figure 10. Antimicrobial activity and behavior of alginate and chitosan films, with and without AgNP, against *E. coli* by disk diffusion method. The different analyses over time (24, 48, and 72 h) are presented in columns, while the rows show the conditions tested: alginate films (on the right dissolved in water and on the left with AgNPs), chitosan films (on the right dissolved in water and on the left with AgNPs).

Table 3. Inhibition zone diameters (mm) obtained against *E. coli* by the disk diffusion method after 24, 48, and 72 h.

	Inhibition Zone Diameters (mm)		
	24 h	**48 h**	**72 h**
Chitosan	6.33 ± 0.34	6.48 ± 0.37	6.99 ± 0.37
Chitosan with AgNP	7.78 ± 0.01	7.92 ± 0.15	8.46 ± 0.23

In the tests performed with the precursor solutions, the alginate solution with AgNPs showed a small inhibition halo, indicating antimicrobial activity (Figure 11). For the chitosan solution, the addition of AgNPs led to an increase in antimicrobial activity (Table 4). The controls confirmed the effectiveness of the antibiotic used as the positive control and showed that water did not interfere with bacterial growth (Table 4 and Figure 11). Additionally, the control containing only AgNPs demonstrated significant antimicrobial activity, attributing the observed effects primarily to silver (Table 4 and Figure 11). The inhibition halos observed at first time (24 h) remained unchanged throughout the test period. The same was true for treatments where it was not possible to visually detect a halo with the naked eye.

Tests with precursor solutions highlighted the critical role of AgNPs in antimicrobial activity, as inhibition halos were observed only in solutions containing nanoparticles [34]. Chitosan solution alone did not exhibit significant antimicrobial effects within the evaluated timeframe, suggesting that its efficacy may depend on the presence of AgNPs. However, as demonstrated in previous studies using the same chitosan concentration—and corroborated here by the absence of microbial growth directly over chitosan films without nanoparticles—chitosan can exhibit inherent antimicrobial properties under certain environmental and structural conditions [35,36].

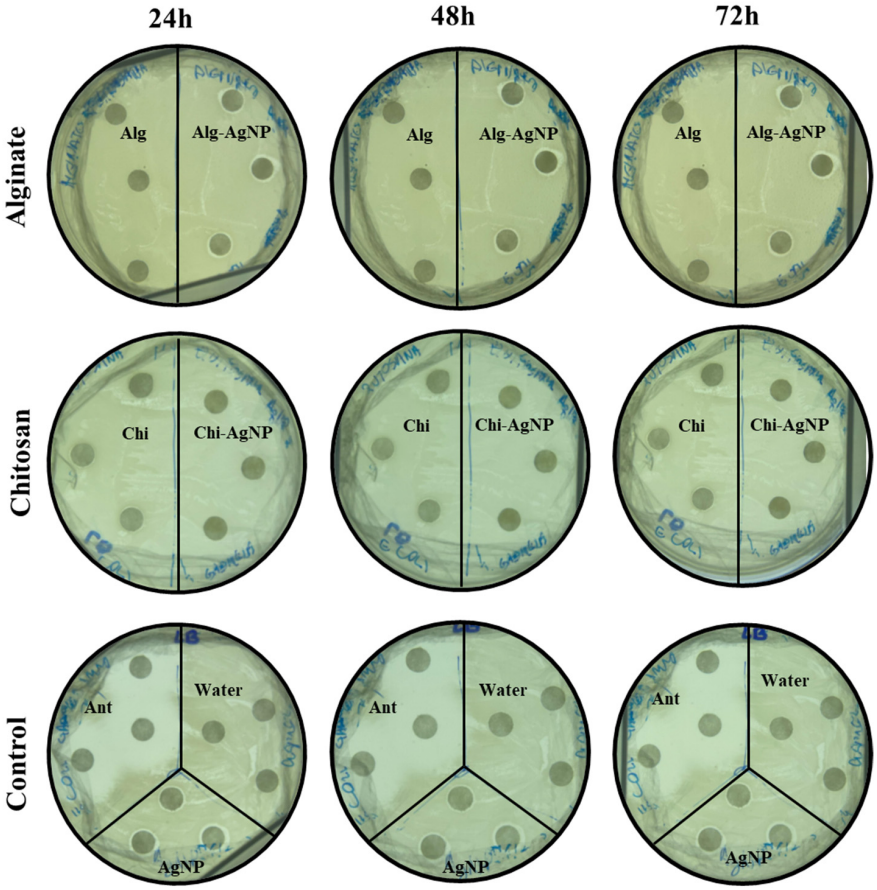

Figure 11. Antimicrobial activity of the precursor solutions of alginate and chitosan films against *E. coli* by the disk diffusion method. The different analyses over time (24, 48, and 72 h) are presented in columns, while the rows display the tested conditions: alginate solutions (right in water and left with silver nanoparticles), chitosan solutions (right in water and left with silver nanoparticles), and finally, the controls.

Table 4. Inhibition zones (mm) for liquid precursor formulations (10 µL per disk) against *E. coli*, measured by the disk diffusion method after 24, 48, and 72 h.

	Inhibition Zone Diameters (mm)		
	24 h	**48 h**	**72 h**
Alginate	6.93 ± 0.11	7.14 ± 0.19	7.01 ± 0.02
Alginate with AgNP	6.91 ± 0.08	7.10 ± 0.16	6.98 ± 0.06
Chitosan	7.09 ± 0.39	7.05 ± 0.20	6.92 ± 0.10
Chitosan with AgNP	7.68 ± 0.88	7.71 ± 1.33	7.61 ± 1.29
Water	8.50 ± 0.91	8.63 ± 1.54	8.54 ± 1.52
AgNP	8.76 ± 0.53	9.25 ± 0.52	9.10 ± 0.61
Antibiotics	8.84 ± 0.72	9.25 ± 0.73	9.10 ± 0.86

Figure 12 shows the ANOVA results and reveals significant differences between the groups ($p < 0.0001$). Tukey's post hoc test showed that most pairwise comparisons were statistically significant, with notable exceptions such as AgNP vs. alginate with AgNP, alginate vs. chitosan, and alginate vs. water, which did not differ significantly ($p > 0.05$). Significant differences were observed between the antibiotic and all other groups, highlighting its distinct efficacy. Additionally, chitosan with AgNP differed significantly from AgNP, alginate with AgNP, and water, emphasizing the impact of AgNP incorporation on the material towards antimicrobial activity. These results suggest that the inclusion of AgNP and the type of material substantially influence the resulting inhibition zone.

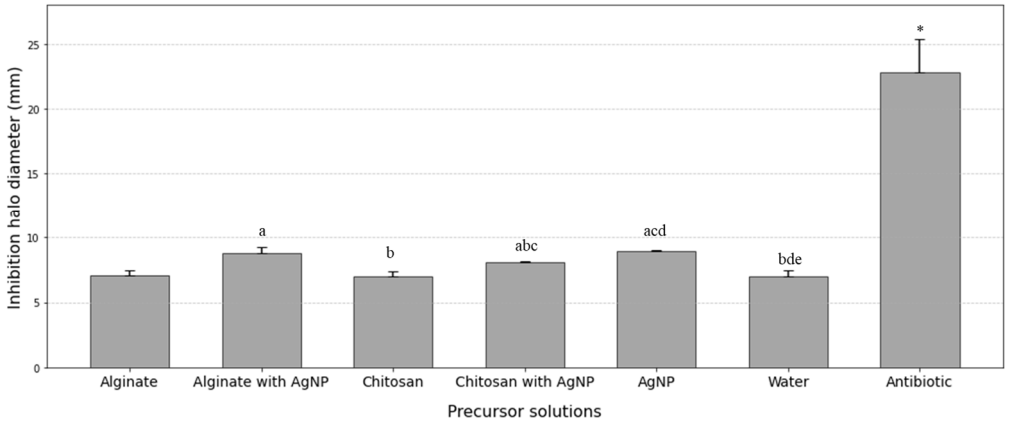

Figure 12. Measurement of the inhibition zone diameters of the film precursor solutions after 24 h. Significant differences are indicated by: (a) alginate; (b) alginate with AgNP; (c) chitosan; (d) chitosan with AgNP; (e) AgNP and (*) antibiotics.

The differentiated antimicrobial activity observed between the films and their corresponding liquid precursors can be explained by the distinct volumes and dispersion behaviors involved in each condition. For the drop-casted films, approximately 40 µL of precursor solution were deposited onto the substrate, resulting in a confined solid layer in which the active compounds remained locally concentrated at the interface with the microbial suspension. In contrast, only 10 µL of each liquid precursor were added to the assay well, and these solutions rapidly dispersed throughout the medium. This increased diffusivity leads to a greater dilution of the active components, thereby decreasing their effective local concentration and reducing antimicrobial efficacy. These differences highlight the importance of considering the physical state and dispersion dynamics of the formulations when interpreting antimicrobial performance.

4. Conclusions

This study provides new insights into the design of antimicrobial biopolymer films by establishing clear structure-property-function relationships in alginate- and chitosan-AgNP systems. Our findings reveal that the film fabrication outcome is critically dependent on the deposition technique, where drop-casting proved fundamentally more effective than spin-coating for forming coherent films on complex, food-grade packaging substrates—a key practical consideration often overlooked in fundamental studies.

DLS analysis indicated relevant changes in hydrodynamic size and ZP of the AgNP after interaction with the biopolymers, suggesting successful polymer coating and potential structural or surface modifications that warrant further investigation. AFM topography showed the formation of relatively homogeneous films, with observable distinctions between films derived from polymers dissolved in water versus those in AgNP suspensions, a finding supported by Raman spectroscopy. Force spectroscopy demonstrated that the addition of AgNP induced distinct nanomechanical alterations in the films, specifically reducing adhesion and elasticity in alginate films while increasing rigidity and adhesion in chitosan-based films. Finally, microbiological tests confirmed the significant antimicrobial activity of both free AgNP and those successfully incorporated into biopolymer films against *E. coli*.

In summary, this study underscores the potential of alginate and chitosan as versatile platforms for developing AgNP-based antimicrobial materials. The choice of biopolymer and fabrication method critically influences the final film's properties. Notably, we demonstrate that chitosan-based films retained structural integrity, making them suitable for applications requiring durability, such as food packaging or wound dressings. Conversely,

alginate films, while undergoing rapid gelation, demonstrated effective antimicrobial release, potentially advantageous for short-term or hydrating applications. More importantly, our integrated characterization approach directly links the opposing electrostatic profiles of the biopolymers in solution to distinct nanomechanical behaviors (reduced adhesion in alginate vs. increased rigidity in chitosan upon AgNP addition) and functional performance in the solid state. This understanding enables a more rational selection of biopolymers and processing techniques for targeted applications. Future studies should focus on optimizing film formation protocols, particularly for challenging substrates, and exploring long-term stability and efficacy in specific application contexts.

Author Contributions: Conceptualization, G.M.d.R.V., J.J.P., C.C.B., and L.P.S.; methodology, G.M.d.R.V., J.J.P., C.C.B., and L.P.S.; formal analysis, G.M.d.R.V.; investigation, G.M.d.R.V.; resources, L.P.S.; data curation, L.P.S.; writing—original draft preparation, G.M.d.R.V.; writing—review and editing, G.M.d.R.V., J.J.P., C.C.B., and L.P.S.; visualization, L.P.S.; supervision, L.P.S.; project administration, L.P.S.; funding acquisition, L.P.S. All authors have read and agreed to the published version of the manuscript.

Funding: This research was funded in part by the Coordenação de Aperfeiçoamento de Pessoal de Nível Superior—Brazil (CAPES—Finance Code 001 and no. 23038.019088/2009-58), Conselho Nacional de Desenvolvimento Científico e Tecnológico (CNPq no. 311825/2021-4, 307853/2018-7, 408857/2016-1, 306413/2014-0, and 563802/2010-3), Fundação de Apoio à Pesquisa do Distrito Federal (FAPDF no. 193.000.445/2008 and 193.000.429/2008), and Empresa Brasileira de Pesquisa Agropecuária (Embrapa no. 10.20.03.009.00.00, 23.17.00.069.00.02, 13.17.00.037.00.00, 21.14.03.001.03.05, 13.14.03.010.00.02, 12.16.04.010.00.06, 22.16.05.016.00.04, 11.13.06.001.06.03, and 10.19.03.054.00). The APC was waived.

Institutional Review Board Statement: Authorization for access to the genetic patrimony (CGEN no. 02001.007580/2014-95). No additional ethical approval was required for this study, as it did not involve human or animal subjects.

Informed Consent Statement: Not applicable.

Data Availability Statement: The original contributions presented in the study are included in the article. Further inquiries can be directed to the corresponding author.

Acknowledgments: This study was developed as part of the graduate course in Biological Sciences (Molecular Biology) at the University of Brasília (UnB), whose academic environment and infrastructure were essential to the completion of this work. During the preparation of this manuscript, the authors used ChatGPT (OpenAI, GPT-5.1) for the purposes of language refinement and assistance in improving clarity and coherence of the text. The authors have reviewed and edited the output and take full responsibility for the content of this publication.

Conflicts of Interest: The authors declare no conflicts of interest. The funders had no role in the design of the study, analysis of data, or decision to publish this manuscript.

Abbreviations

The following abbreviations are used in this manuscript:

AgNP	Silver Nanoparticles
AFM	Atomic force microscopy
DLS	Dynamic light scattering
EM	Electrophoretic mobility
HD	Hydrodynamic diameter
LB	Luria-Bertani
PdI	Polydispersity index
UV	Ultraviolet
ZP	Zeta potential

References

1. Polívková, M.; Kolář, M.; Šteflová, M.; Pavlík, M.; Rybár, P.; Dubový, P.; Kaderka, R.; Hálek, J. Antimicrobial treatment of polymeric medical devices by silver nanomaterials and related technology. *Int. J. Mol. Sci.* **2017**, *18*, 419. [CrossRef]
2. Zhou, G.; Xu, R.; Groth, T.; Wang, Y.; Yuan, X.; Ye, H.; Dou, X. The combination of bioactive herbal compounds with biomaterials for regenerative medicine. *Tissue Eng. Part B Rev.* **2024**, *30*, 607–630. [CrossRef] [PubMed]
3. Campbell, I.R.; Lin, M.Y.; Iyer, H.; Parker, M.; Fredricks, J.L.; Liao, K.; Jimenez, A.M.; Grandgeorge, P.; Roumeli, E. Progress in sustainable polymers from biological matter. *Annu. Rev. Mater. Res.* **2023**, *53*, 81–104. [CrossRef]
4. Ebnesajjad, S. (Ed.) *Handbook of Biopolymers and Biodegradable Plastics: Properties, Processing and Applications*; William Andrew: Norwich, NY, USA, 2012.
5. Baranwal, J.; Barse, B.; Fais, A.; Delogu, G.L.; Kumar, A. Biopolymer: A sustainable material for food and medical applications. *Polymers* **2022**, *14*, 983. [CrossRef]
6. Taheri, S.; Vasilev, K.; Majewski, P. Silver nanoparticles: Synthesis, antimicrobial coatings, and applications for medical devices. *Recent Pat. Mater. Sci.* **2015**, *8*, 166–175. [CrossRef]
7. Porter, G.C.; Schwass, D.R.; Tompkins, G.R.; Bobbala, S.K.; Medlicott, N.J.; Meledandri, C.J. AgNP/Alginate nanocomposite hydrogel for antimicrobial and antibiofilm applications. *Carbohydr. Polym.* **2021**, *251*, 117017. [CrossRef] [PubMed]
8. Lee, K.Y.; Mooney, D.J. Alginate: Properties and biomedical applications. *Prog. Polym. Sci.* **2012**, *37*, 106–126. [CrossRef]
9. Rinaudo, M. Chitin and chitosan: Properties and applications. *Prog. Polym. Sci.* **2006**, *31*, 603–632. [CrossRef]
10. Elieh-Ali-Komi, D.; Hamblin, M.R. Chitin and chitosan: Production and application of versatile biomedical nanomaterials. *Int. J. Adv. Res.* **2016**, *4*, 411–427.
11. Raus, R.A.; Nawawi, W.M.F.W.; Nasaruddin, R.R. Alginate and alginate composites for biomedical applications. *Asian J. Pharm. Sci.* **2021**, *16*, 280–306. [CrossRef] [PubMed]
12. Swarupa, S.; Thareja, P. Techniques, applications and prospects of polysaccharide and protein based biopolymer coatings: A review. *Int. J. Biol. Macromol.* **2024**, *266*, 131104. [CrossRef] [PubMed]
13. Bhattacharjee, S. DLS and zeta potential-What they are and what they are not? *J. Control. Release* **2016**, *235*, 337–351. [CrossRef]
14. Priya, G.; Shanthi, N.; Pavithra, S.; Sangeetha, S.; Murugesan, S.; Shyamalagowri, S. Modern analytical approach in biopolymer characterization. *Phys. Sci. Rev.* **2024**, *9*, 1149–1170. [CrossRef]
15. Lee, J.H.; Jeong, D.; Kanmani, P. Study on physical and mechanical properties of the biopolymer/silver based active nanocomposite films with antimicrobial activity. *Carbohydr. Polym.* **2019**, *224*, 115–159. [CrossRef]
16. Bonatto, C. Development and Evaluation of In Vitro and In Vivo Biological Activities of Silver Micro- and Nanoparticles Obtained by Green Synthesis Using Plants from the Cerrado. Ph.D. Thesis, University of Brasília, Brasília, Brazil, 2016.
17. Freire, A.M. Development of a Low-Cost Spin-Coater and Assessment of Alginate Film Production. Master's Thesis, University of Brasília, Brasília, Brazil, 2024.
18. Tetra Pak. Material de Embalagem. Available online: https://www.tetrapak.com/pt-br/solutions/packaging/packaging-material (accessed on 28 November 2024).
19. Al-Gunaid, T.A.; Albaroudi, A.; Alhamdany, A.; Al-Sakkaf, A.; Al-Mahrami, R.; Ahmed, I.; Rashid, K.A. Enhancement of adhesion characteristics of low-density polyethylene using atmospheric plasma initiated-grafting of polyethylene glycol. *Polymers* **2021**, *13*, 1309. [CrossRef]
20. Martínez-Cisterna, D.; Chen, L.; Bardehle, L.; Hermosilla, E.; Tortella, G.; Chacón-Fuentes, M.; Rubilar, O. Chitosan-Coated Silver Nanocomposites: Biosynthesis, Mechanical Properties, and Ag+ Release in Liquid and Biofilm Forms. *Int. J. Mol. Sci.* **2025**, *26*, 4130. [CrossRef]
21. Campos-Vallette, M.M.; Chandía, N.P.; Clavijo, E.; Leal, D.; Matsuhiro, B.; Osorio-Román, I.O.; Torres, S. Characterization of sodium alginate and its block fractions by surface-enhanced Raman spectroscopy. *J. Raman Spectrosc.* **2010**, *41*, 758–763. [CrossRef]
22. Salomonsen, T.; Jensen, H.M.; Stenbæk, D.; Engelsen, S.B. Rapid determination of alginate monomer composition using Raman spectroscopy and chemometrics. *Gums Stabil. Food Ind.* **2008**, *14*, 543–551. [CrossRef]
23. Nirmala, R.; Il, B.W.; Navamathavan, R.; El-Newehy, M.H.; Kim, H.Y. Preparation and characterization of anisotropic chitosan nanofibers via electrospinning. *Macromol. Res.* **2011**, *19*, 345–350. [CrossRef]
24. Zając, A.; Hanuza, J.; Wandas, M.; Dymińska, L. Determination of N-acetylation degree in chitosan using Raman spectroscopy. *Spectrochim. Acta A Mol. Biomol. Spectrosc.* **2015**, *134*, 114–120. [CrossRef]
25. Simpliciano, C.; Clark, L.; Asi, B.; Chu, N.; Mercado, M.; Diaz, S.; Mobed-Miremadi, M. Cross-linked alginate film pore size determination using atomic force microscopy and validation using diffusivity determinations. *J. Surf. Eng. Mater. Adv. Technol.* **2013**, *3*, 1–12. [CrossRef]
26. Lewandowska, K.; Szulc, M. Rheological and film-forming properties of chitosan composites. *Int. J. Mol. Sci.* **2022**, *23*, 8763. [CrossRef]
27. Sarwar, M.S.; Huang, Q.; Ghaffar, A.; Abid, M.A.; Zafar, M.S.; Khurshid, Z.; Latif, M. A smart drug delivery system based on biodegradable chitosan/poly (allylamine hydrochloride) blend films. *Pharmaceutics* **2020**, *12*, 131. [CrossRef]

28. Badita, C.R.; Aranghel, D.; Burducea, C.; Mereuta, P.J. Characterization of sodium alginate based films. *Rom. J. Phys.* **2020**, *65*, 1–8.
29. Butt, H.-J.; Cappella, B.; Kappl, M. Force measurements with the atomic force microscope: Technique, interpretation and applications. *Surf. Sci. Rep.* **2005**, *59*, 1–152. [CrossRef]
30. Li, J.; Wu, Y.; He, J.; Huang, Y. A new insight to the effect of calcium concentration on gelation process and physical properties of alginate films. *J. Mater. Sci.* **2016**, *51*, 5791–5801. [CrossRef]
31. Giz, A.S.; Berberoglu, M.; Bener, S.; Aydelik-Ayazoglu, S.; Bayraktar, H.; Alaca, B.E.; Catalgil-Giz, H. A detailed investigation of the effect of calcium crosslinking and glycerol plasticizing on the physical properties of alginate films. *Int. J. Biol. Macromol.* **2020**, *148*, 49–55. [CrossRef] [PubMed]
32. Kubyshkin, A.; Chegodar, D.; Katsev, A.; Petrosyan, A.; Krivorutchenko, Y.; Postnikova, O. Antimicrobial effects of silver nanoparticles stabilized in solution by sodium alginate. *Biochem. Mol. Biol. J.* **2016**, *2*, 13. [CrossRef] [PubMed]
33. Kanniah, P.; Chelliah, P.; Thangapandi, J.R.; Gnanadhas, G.; Mahendran, V.; Robert, M. Green synthesis of antibacterial and cytotoxic silver nanoparticles by Piper nigrum seed extract and development of antibacterial silver based chitosan nanocomposite. *Int. J. Biol. Macromol.* **2021**, *189*, 18–33. [CrossRef] [PubMed]
34. Kailasa, S.K.; Park, T.J.; Rohit, J.V.; Koduru, J.R. Antimicrobial activity of silver nanoparticles. In *Nanoparticles in Pharmacotherapy*; William Andrew Publishing: Norwich, NY, USA, 2019; pp. 461–484.
35. Foster, L.J.R.; Butt, J. Chitosan films are NOT antimicrobial. *Biotechnol. Lett.* **2011**, *33*, 417–421. [CrossRef]
36. Hosseinnejad, M.; Jafari, S.M. Evaluation of different factors affecting antimicrobial properties of chitosan. *Int. J. Biol. Macromol.* **2016**, *85*, 467–475. [CrossRef] [PubMed]